analytical chemistry

pubs.acs.org/ac Article

Ultrasensitive Nucleic Acid Assay Based on AIE-Active Polymer Dots with Excellent Electrochemiluminescence Stability

Nan Zhang,[§] Hang Gao, Yi-Lei Jia, Jian-Bin Pan,* Xi-Liang Luo, Hong-Yuan Chen, and Jing-Juan Xu*

Cite This: *Anal. Chem.* 2021, 93, 6857−6864 Read Online

ACCESS | Metrics & More | Article Recommendations | Supporting Information

ABSTRACT: Aggregation-induced emission (AIE) active Pdots are attractive nanomaterials applied in electrochemiluminescence (ECL) fields, while the irreversible redox reaction of these Pdots is a prevailing problem, resulting in instability of ECL emission. Herein, we first designed and synthesized an AIE-active Pdot with reversible redox property, which contains a tetraphenylethene derivate and benzothiadiazole (BT) to achieve stable ECL emission. BT has a good rigid structure with excellent electrochemical behaviors, which is beneficial for avoiding the destruction of the conjugated structure as much as possible during the preparation of Pdots, thus maintaining good redox property. The tetraphenylethene derivate, as a typical AIE-active moiety, provides a channel for highly efficient luminescence in the aggregated states. The Pdots exhibited reversible and quasi-reversible electrochemical behaviors during cathodic and anodic scanning, respectively. The stable annihilation, reductive−oxidative, and oxidative−reductive ECL signals were observed. Subsequently, we constructed an ultrasensitive ECL biosensor based on the oxidative−reductive ECL mode for the detection of miRNA-21 with a detection limit of 32 aM. This work provides some inspiration for the future design of ECL materials featuring AIE-active property and stable ECL emission.

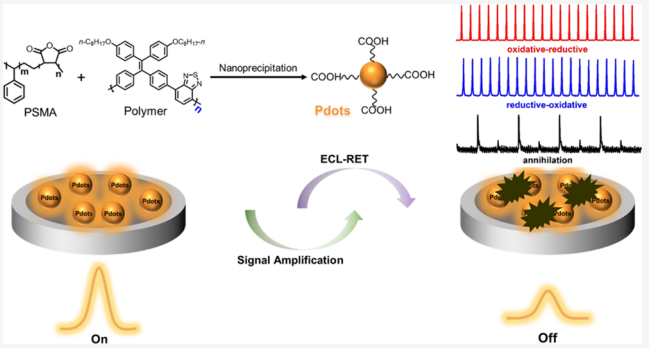

Aggregation-induced emission (AIE) is a luminescence process, where luminophores are weak or show no emission as molecular species, while show strong emission as aggregates.[1] Owing to the high luminescence efficiency in aggregate states of AIE-active materials, they have achieved considerable attention because of their applications in fluorescence imaging,[2] biosensing,[3] chiral recognition,[4] and organic light-emitting diodes (OLEDs).[5] To meet the ever-increasing demand for various fields, diverse nanomaterials with AIE-active properties have emerged, including nanocrystals,[6] metal clusters,[7] organic dots,[8] and polymer dots (Pdots).[9] Among them, with the development of aggregation-induced electrochemiluminescence (AIECL),[10−15] due to their advantages of excellent structural modification, good biocompatibility, and high luminescence intensity in aggregated states, AIE-active Pdots have been gradually investigated in ECL fields.[16] Until now, these reported AIE-active Pdots could be divided into several categories according to the molecular composition, for example, iridium(III)-containing Pdots,[17−19] boron-based Pdots,[20] and fluorene- or carbazole-based Pdots.[21] While they exhibit strong ECL signals, most of them show poor stability of ECL emission. The reason for instability might be ascribed to the irreversible electrochemical behaviors of Pdots, although partial polymers show reversible redox reactions. This may be due to the collapse and curling of the conjugated polymer during the preparation of Pdots under ultrasonic conditions,[22] causing planarity of the conjugated backbone to be destroyed and the electronic energy level to be reorganized, resulting in changes in electrochemical redox properties, where the phenomenon is also common in other organic nanosystems.[23] The negative effect limits their application in the field of actual sensing and detection. Therefore, it is necessary and important to design AIE-active Pdots with excellent redox reversibility to obtain good stability of ECL emission.

In this regard, recently, our group introduced traces of an iridium(III) complex into AIE-active Pdots, which exhibited good stability of ECL emission.[17] It might involve the redox reaction of the iridium(III) complex with excellent electrochemical properties during an ECL process, where ECL emission originated from intramolecular electron transfer between the conjugated backbone of Pdots and the iridium(III) complex. On the other hand, to overcome this problem of destruction of the conjugated backbone as much as possible

Received: March 2, 2021
Accepted: April 13, 2021
Published: April 23, 2021

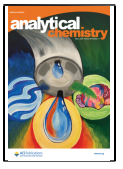

https://doi.org/10.1021/acs.analchem.1c00947
Anal. Chem. 2021, 93, 6857−6864

Scheme 1. Synthesis Route of the Polymer and Preparation of Pdots Used in This Work

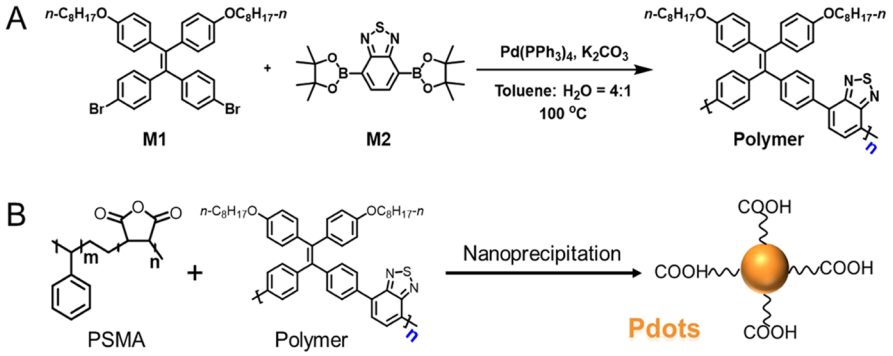

during the preparation of Pdots, introducing rigid structures into polymers could be a better method. Owing to the good structural modification and rigidity, as well as outstanding electrochemical property, benzothiadiazole (BT), as an important electron acceptor, has been extensively applied in the photoelectric fields, such as OLEDs,[24] organic field-effect transistors,[25] organic solar cells,[26] and ECL.[27] Construction of a molecule with the core of BT exhibits remarkable redox reversibility in the aggregated states, which will also benefit the notable stability of ECL emission. Until now, to our best knowledge, the study of BT-based Pdots focuses on poly[(9,9-dioctylfuorenyl-2,7-diyl)-*alt-co*-(1,4-benzo[*c*][1,2,5]-thiadiazole)] (PFBT).[28,29] However, not to be ignored, the good structural planarity of BT can easily lead to aggregation caused by quenching effects due to $\pi-\pi$ stacking, which decreases the luminescence efficiency. Herein, through a distorted structure of the electron donor linked to BT, AIE-active Pdots is conveniently designed to solve this problem.

In this paper, we synthesized poly[4-(4-(2,2-bis(4-(octyloxy)phenyl)-1-phenylvinyl)phenyl)benzo[*c*][1,2,5]-thiadiazole] and converted it into Pdots by a nanoprecipitation method. The Pdots consisted of a tetraphenylethene derivate, a typical AIE-active moiety, and BT, which was not only beneficial to strong ECL emission in the aggregated states but also provided good stability to ECL intensity with a relative standard deviation (RSD) of 0.6%. As we all know, the stability of luminescent materials is crucial to the construction of biosensors. In view of the excellent ECL stability of the novel Pdots prepared in this work, we used them to develop an ECL biosensor for sensitive detection of miRNA-21. To achieve the purpose of high sensitivity, our sensor design combined two recycling amplification strategies, duplex-specific nuclease (DSN)-assisted target recycling amplification and catalytic hairpin assembly (CHA) approaches. In addition, the electrochemiluminescence resonance energy transfer (ECL-RET) strategy was also applied in our design while using Pdots as a donor and a black hole quencher (BHQ) as an acceptor. With these efforts, a novel and sensitive ECL biosensor for miRNA-21 detection with a detection limit of 32 aM was achieved.

EXPERIMENTAL SECTION

Materials, Reagents, and Apparatus. The detailed information is listed in the Supporting Information.

Synthesis of the Conjugated Polymer. The polymer was synthesized according to Scheme 1A. A mixture of 4,4′-(2,2-bis(4-(octyloxy)phenyl)ethene-1,1-diyl)bis-(bromobenzene) (**M1**, 119.5 mg, 0.16 mmol), 4,7-bis(4,4,5,5-tetramethyl-1,3,2-dioxaborolan-2-yl)benzo[*c*][1,2,5]thiadiazole (**M2**, 63.4 mg, 0.16 mmol), $Pd(PPh_3)_4$ (19 mg, 1.6% mmol), and K_2CO_3 (221 mg, 1.6 mmol) in PhMe/H_2O (8 mL:2 mL) in a Schlenk tube was stirred at 100 °C under an argon atmosphere. After reaction for 72 h, bromobenzene (3.1 mg, 0.02 mmol) was added for a period of 2 h and then phenylboronic acid (4.8 mg, 0.04 mmol) was added for another 2 h. After the reaction was completed, the resulting polymers were purified by being precipitated in methanol twice as a yellow solid (96.0 mg, 83%).

Preparation of Polymer Dots (Pdots). The Pdots were prepared by the nanoprecipitation method according to a previous literature.[30] In brief, 200 μL of 1.0 mg/mL polymers in THF and 40 μL of 1.0 mg/mL poly(styrene-*co*-maleicanhydride) (PSMA) in THF were mixed and then diluted to 2 mL with THF. After ultrasonically degassed for 3 min under room temperature (Elmasonic P30H, Germany), the mixture was quickly added to 10 mL of Milli-Q water in a bath sonicator (120 W, 37 kHz) for 5 min. The THF solvent was removed by rotary evaporation under vacuum, followed by filtration through a 0.22 μm poly(ether sulfones) (PES) syringe filter (Millex-GP Filter, Millipore) to obtain the Pdot stock solution in H_2O with 100 μg/mL. The role of PSMA is to use its amphiphilic properties to obtain the hydrophilic carboxyl groups on the surface of Pdots (the detailed process is shown in Scheme 1B).

Electrochemical Measurements. The cyclic voltammetry measurement of Pdots was conducted with a three-electrode system. It was conducted with a glass carbon electrode (GCE, diameter 3 mm), a platinum wire counter electrode, and a Ag/$AgNO_3$ (10 mM in CH_3CN solution) nonaqueous quasi-reference electrode. The quasi-reference electrode was calibrated with a saturated Ag/AgCl electrode by comparing redox potentials of ferrocene/ferrocenium (Fc/Fc^+).

DSN-Assisted MiRNA Recycling Amplification. It was performed in 20 μL of reaction mixture containing 1× DSN master buffer (50 mM Tris−HCl (pH 8.0), 5 mM $MgCl_2$, and 1 mM DTT), 0.2 U of DSN, different concentrations of miRNA-21, and 10 μM hairpin H_0, and the obtained reaction mixture is then incubated at 50 °C for 1 h. Then, 10 μL of DSN stop solution was added. The final solution contained different amounts of report DNA and applied to the next step of amplification.

Procedure for ECL Detection of MiRNAs. Prior to ECL measurement, a glassy carbon electrode (GCE, diameter of 3 mm) was polished with 1.0, 0.3, and 0.05 μm of Al_2O_3 powder and ultrasonically cleaned with ethanol and water alternately. A volume of 10 μL of 5 μg/mL Pdots was cast on the surface of the GCE and dried at room temperature. Then, the above

https://doi.org/10.1021/acs.analchem.1c00947
Anal. Chem. 2021, 93, 6857−6864

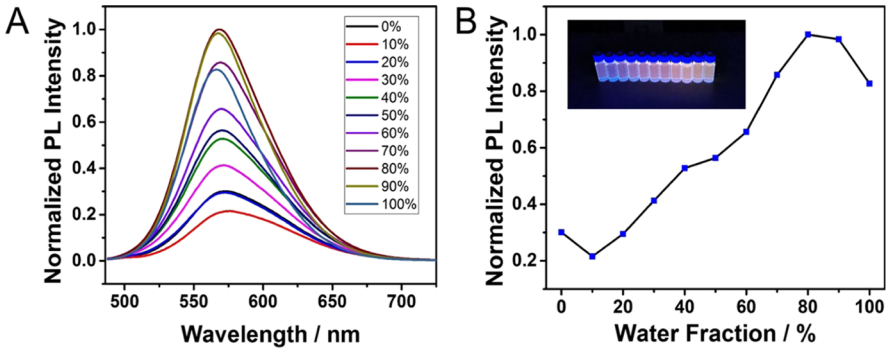

Figure 1. (A) Fluorescence spectra of the polymer with different water volume fractions. (B) Corresponding PL peak intensity changes of the polymer with different water fractions in (A) (the inset image shows luminescence photographs of the polymer in different solvents according to (A), which were taken under 365 nm UV illumination).

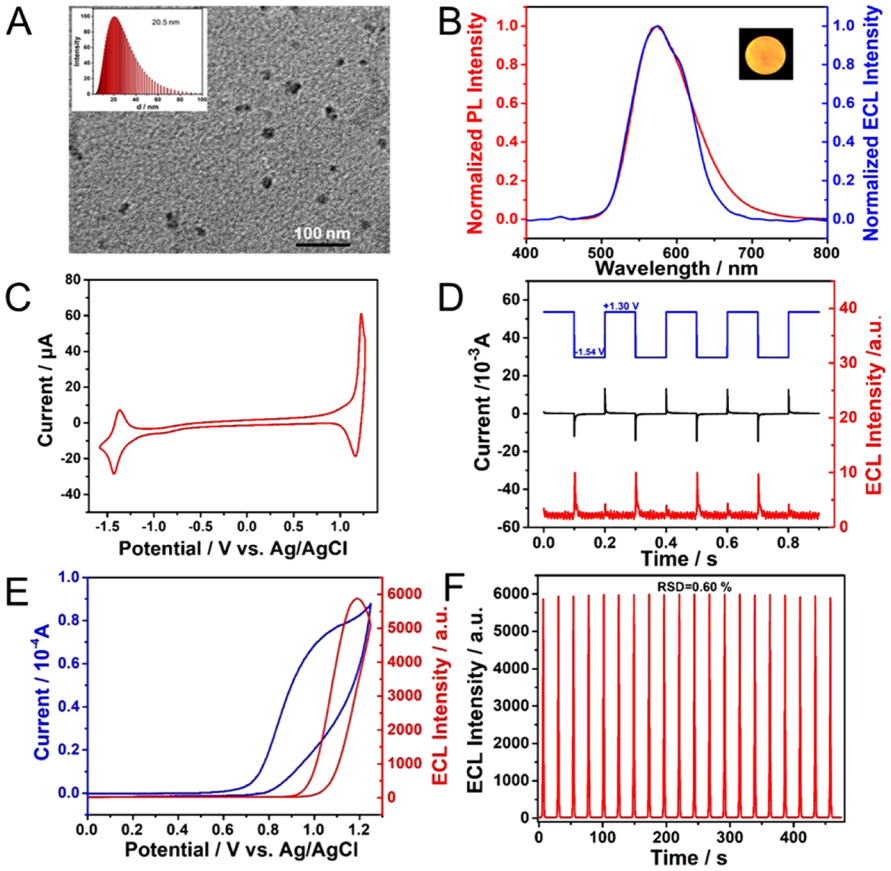

Figure 2. (A) TEM image of Pdots; accelerating voltage, 200 kV (the inset image shows the hydrodynamic diameter of Pdots measured by DLS). (B) Normalized photoluminescence spectrum (red line) of Pdots and normalized ECL emission spectrum of Pdots in the presence of TPrA (the inset shows the ECL emission image of the Pdots by CCD). (C) Cyclic voltammogram of Pdots in the CH_3CN solution using 0.1 M TBAPF6 as an electrolyte at a scan rate of 100 mV/s. (D) Transient profiles for potential magnitude (blue), current value (black), and ECL intensity (red) of Pdots in 0.1 M PBS (voltage of PMT, 700 V). (E) CV diagram (blue curve) and ECL profile (red curve) of 5 μg/mL Pdots containing 25 mM TPrA (PMT voltage, 600 V). (F) Stability test of oxidative−reductive ECL for Pdot-modified GCE under 20 cyclic potential scans (voltage of PMT, 600 V).

Pdot-modified GCE was immersed in the cross-linking agent (20 mM 1-ethyl-3-(3-dimethylaminopropyl)carbodiimide and 10 mM *N*-hydroxysuccinimide) at room temperature for 30 min. Then, H_1 (10 μL, 10 μM) was incubated onto the Pdots layer with active carboxyl groups at 4 °C overnight. After the nonspecific sites were blocked with MCH (1.0 mM) for 40 min at room temperature, the prepared solution containing different concentrations of report DNA (10 μL) was incubated on the electrode for 2 h at 37 °C, and then, the H_2-BHQ composite (10 μL, 10 μM) was incubated on the electrode for 2 h at 37 °C. Also, after each step of modification, the excess DNA and other molecules were washed away with ultrapure water. The ECL response of the modified electrodes was detected in 5.0 mL of phosphate-buffered saline (0.10 M PBS, pH 7.4) containing 25 mM tri-*n*-propylamine (TPrA) at a potential range of 0−1.25 V and a scan rate of 200 mV/s. The voltage of the photomultiplier tube (PMT) was set to 700 V unless specifically mentioned.

https://doi.org/10.1021/acs.analchem.1c00947
Anal. Chem. 2021, 93, 6857−6864

RESULTS AND DISCUSSION

Characterization of the Polymer. In this work, we synthesized a novel polymer with a tetraphenylethene derivate and a BT structure, which is conducive to enhancing luminescence efficiency in the aggregated states and improving the electrochemical redox reversibility of the system. The ^{1}H NMR spectra of polymer are shown in Figure S1. The NMR peak information was provided below the figure, which confirmed that the polymer was successfully synthesized.

First, the aggregation behavior of the polymer in THF/H_2O mixtures with different ratios was investigated (Figure 1A and B). With the water fraction (f_w) increasing from 0 to 10%, the PL intensity decreased, which might be due to transformation to the twisted intramolecular charge transfer (TICT) state generally existed among donor−acceptor structures. With the continuous increase of H_2O fraction, the fluorescence intensity gradually increased and attained peak when the H_2O fraction was up to 80%, indicative of a typical AIE property. Afterward, the emission intensity showed a slight decrease as f_w increased from 80 to 99%, which might be caused by the solubility decline in excess of poor solvents. The UV−vis absorption of the polymer is shown in Figure S2A. The intense absorption band at 320 nm was assigned to the $\pi-\pi^*$ transition of the entire conjugated backbone, while the other absorption band in the visible range of 420 nm could be ascribed to the intramolecular charge transfer (ICT) process.

Characterization of Pdots. The morphology of the Pdots was obtained by transmission electron microscopy (TEM); the diameter of Pdots was near 16 nm (Figure 2A), and its hydration particle size was about 20.5 nm, as measured with the dynamic light scattering (DLS) method, which was consistent with the TEM results. The absorbance spectra of Pdots are shown in Figure S2B, and the attribution of the corresponding peak was similar to the polymer in Figure S2A. The ζ-potential of the Pdots was −15.8 mV, which was ascribed to the carboxyl on the surface of the Pdots. Then, we integrated and studied the PL and ECL spectra of Pdots. It was reported that the comparison between ECL and PL spectra of NPs was a good way to investigate whether the NPs had significant surface traps because ECL was mainly characterized by surface state transitions as compared with PL.[31] The spectra are displayed in Figure 2B; we can observe a strong PL emission peak at 573 nm, which was close to the ECL emission centered at 575 nm. The result showed that our Pdots had no deep surface traps, and the ECL mode was band gap ECL emission.[32] Also, the inset shows the ECL image of the Pdots captured by a charge-coupled device (CCD), which displayed a bright orange-red color corresponding to the peak of ECL spectra at 575 nm. In addition, as shown in Figure S3, the phosphorescent lifetime of the Pdots was 2.45 ns and the absolute PL quantum yield was 25.43%. The relevant characterization data are summarized in Table S2.

Before conducting ECL research, cyclic voltammetry (CV) was performed to study the electrochemical performance of the Pdots in the CH_3CN solution using 0.1 M $TBAPF_6$ as a supporting electrolyte. As displayed in Figure 2C, the Pdots showed a couple of quasi-reversible redox peaks at a formal potential of 1.194 V with an onset potential of 0.908 V, which might be assigned to the entire conjugated structures because of electron delocalization of the highest occupied molecular orbital (HOMO).[33] During the process of negative scanning, a reversible redox peak was also observed at a formal potential of −1.397 V with an onset potential of −1.185 V, which could be ascribed to the reduction of the BT group.[27]

After obtaining the electrochemical redox data of Pdots, the transient ECL performance was studied by a potential step pulse method between 1.30 and −1.54 V vs Ag/AgCl with a pulse width of 0.1 s. The signals of ECL and current are shown in Figure 2D. It was noted that the ECL intensity in both cases was relatively stable when the direction of the potential step was different. Also, the ECL intensity was much stronger when the potential switched from 1.30 V to −1.54 V compared with the reversal step, indicating that the radical cation ($Pdots^{\bullet+}$) was more stable than the radical anion ($Pdots^{\bullet-}$).

Next, oxidative−reductive and reductive−oxidative ECL properties of the Pdots with corresponding coreactants were investigated. The results are shown in Figures 2E and S4; in comparison to reductive−oxidative ECL, the Pdots showed more significant signals during the process of oxidation−reduction, possibly because the radical cation ($Pdots^{\bullet+}$) was more stable. To improve the sensitivity of the biosensor and consider the application in reality, we investigated the oxidative−reductive ECL in detail. As revealed in Figure 2E, in the curve of cyclic voltammetry (blue line), an oxidative peak potential at 1.015 V was observed with an onset potential of 0.622 V, which was consistent with the redox behaviors of TPrA in the PBS (Figure S5). The redox wave of Pdots was hidden by the strong and irreversible oxidation wave of TPrA. The ECL emission peak was observed at 1.18 V with an onset potential of 0.913 V (red line), which was basically consistent with the electrochemical behaviors shown in Figure 2C. On the basis of previous research,[20,21,34] we speculated the possible ECL emission mechanism of Pdots/TPrA as follows:

$$TPrA - e^- \rightarrow TPrAH^{\bullet+} \quad (1)$$

$$TPrA^{\bullet+} - H^+ \rightarrow TPrA^{\bullet} \quad (2)$$

$$Pdots - e^- \rightarrow Pdots^{\bullet+} \quad (3)$$

$$Pdots^{\bullet+} + TPrA^{\bullet} \rightarrow Pdots^* + Pr_2N^+HC = CH_2CH_3 \quad (4)$$

$$Pdots^* \rightarrow Pdots + h\nu \quad (5)$$

Moreover, to distinctly demonstrated the ECL performance of the Pdots, commercial ECL reagent $[Ru(bpy)_3]^{2+}$ was chosen as a reference. The relative quantum efficiency was estimated by eq 6[35−37]

$$\varnothing_x = \varnothing_{st}\left(\frac{\int_0^t I\,dt}{\int_0^t i\,dt}\right)_x \Big/ \left(\frac{\int_0^t I\,dt}{\int_0^t i\,dt}\right)_{st} \quad (6)$$

In the above equation, $\varnothing_x$ represents the ECL relative quantum efficiency of the Pdots. I and i stand for the ECL intensity and current value, respectively. $\varnothing_{st}$ stands for the ECL efficiency of 0.1 mM $[Ru(bpy)_3]^{2+}$ in 0.1 M PBS containing 25 mM TPrA, and this value was set as 1. The result of $\varnothing_x$ was calculated as 0.1. It demonstrated that the Pdots had an acceptable ECL relative quantum efficiency, which is 10% that of the standard system of $[Ru(bpy)_3]^{2+}$/TPrA. It was one of the higher values obtained until now (Table S3). As shown in Figure 2F, the Pdots exhibited good ECL stability for the consecutive scans of 20 cycles with an RSD of 0.6%. The ECL stability of the reductive−oxidative process was also conducted, and the result is shown in Figure S6. Both types of ECL emissions had good stability, which were benefited from the good electrochemical

https://doi.org/10.1021/acs.analchem.1c00947
Anal. Chem. 2021, 93, 6857−6864

Scheme 2. Schematic Diagram and Principle for miRNA-21 Detection by the Immunosensor

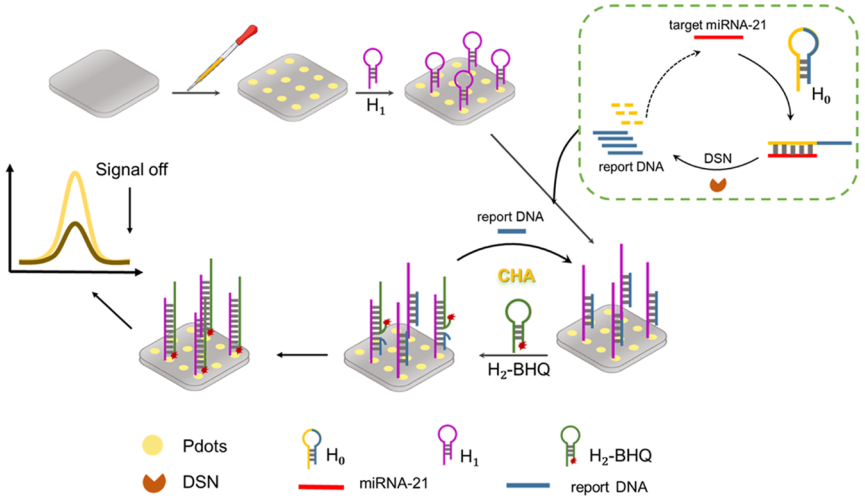

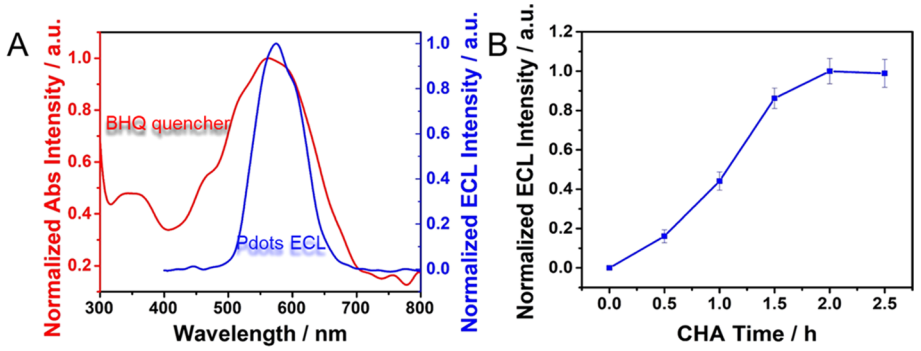

Figure 3. (A) Absorbance spectrum of the BHQ quencher (red line) and ECL emission spectrum of Pdots (blue line). (B) Optimization of the CHA reaction time.

reversibility of Pdots under positive and negative voltage scanning, as shown in Figure 2C. Also, these phenomena were consistent with the transient step experiment results in Figure 2D (red line). To achieve a better detection effect, different coreactants were used for the ECL test. Under the same condition, the performance of TPrA was more excellent compared with triethylamine (TEA) and 2,2′-(butylimino)-diethanol (BDEA) (Figure S7). We further optimized the concentration of TPrA, and the maximum ECL intensity was obtained with 25 mM TPrA (Figure S8).

Detection Principle of the ECL Biosensor. Based on the above discussion, it can be seen that Pdots had good ECL stability and the luminous intensity in the oxidative−reductive mode was most remarkable, so they were suitable as a substrate material of ECL sensors. Taking into consideration the high ECL intensity and suitable emission wavelength range of Pdots, they were applicable for use as an ECL donor, while BHQ molecules were used as an ECL acceptor to construct an ECL-RET biosensor for the sensitive detection of miRNA-21, where BHQ could quench the ECL emission of Pdots. The fabrication procedure and the detection principle are described in Scheme 2. As shown in the green dashed box of Scheme 2, in the presence of DSN enzyme, a small amount of target miRNA-21 corresponds to a large amount of report DNA, which realized the first step of amplification.[38,39] As for another strategy, CHA could achieve exponential amplification of target DNA with a negligible background at high speeds.[40−42] As we can see, the more the report DNA, the more the H_2-BHQ was captured at the electrode. In short, with the increase of the target, the BHQ quencher gradually increased, while the ECL intensity gradually decreased. Accordingly, the concentration of miRNA-21 could be measured by monitoring the change in the ECL intensity of the sensor.

To verify the rationality of our designed signal recycling amplification system, polyacrylamide gel electrophoresis was performed to monitor the DSN assistant recycling and CHA reaction. From Figure S9, in the presence of miRNA-21, H_0 hybridized with it and a new band appeared (lane c). After digestion by the DSN enzyme, the report DNA was produced (lane d). For the CHA reaction, as can be seen in Figure S10, in the absence of report DNA, H_1 could hardly hybridize with H_2 even after an annealing process (lane e). When report DNA was added, it immediately hybridized with H_1 (lane c) and catalyzed the hybridization of H_1 and H_2 (lane d). Also, the clear band of report DNA further indicated that the report DNA could be replaced by H_2, released, and reused for multiple reaction cycles.

To verify the feasibility of our designed ECL-RET strategy between a Pdots donor and a BHQ quencher, the absorbance spectrum of BHQ-modified DNA and the ECL spectrum of Pdots were studied. As shown in Figure 3A, BHQ had a broad range of absorption between 400 and 700 nm (red line) and the ECL emission of Pdots was located at 500−670 nm (blue line). It was apparent that the absorption spectrum of BHQ overlapped well with the ECL emission spectrum of the Pdots, so the feasibility of the ECL-RET strategy was demonstrated.

https://doi.org/10.1021/acs.analchem.1c00947
Anal. Chem. 2021, 93, 6857−6864

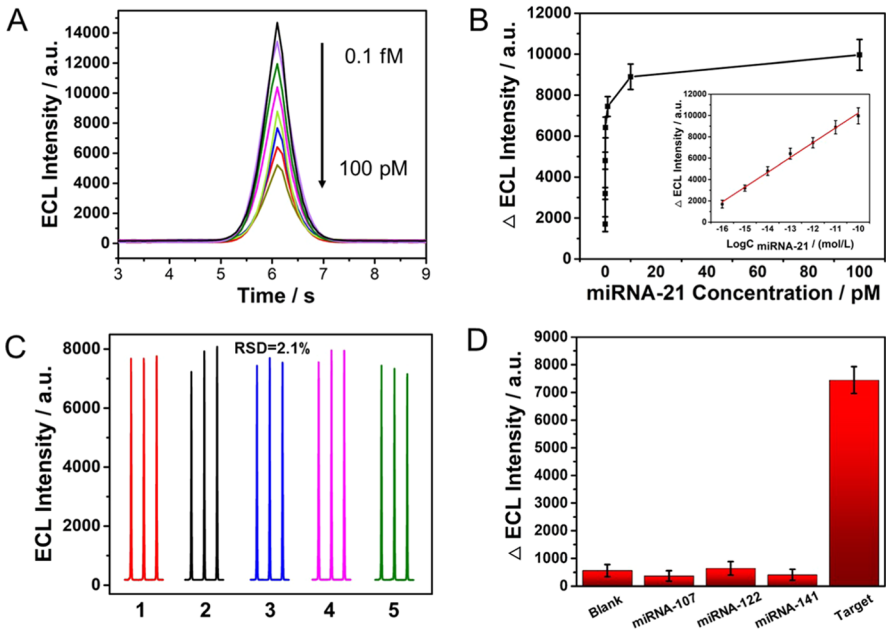

Figure 4. (A) ECL profiles of the immunosensor incubated with varying concentrations of miRNA-21 in the range from 0.1 fM to 100 pM. (B) Correlation between the ΔECL intensities and the concentrations of miRNA-21 from 0.1 fM to 100 pM. The inset shows the linear correlation diagram. (C) Reproducibility of the ECL biosensor for detection of 1 pM miRNA-21. (D) Selectivity of the developed biosensor for the target miRNA-21 (1 pM) detection against the blank assay and other miRNA sequences at 10 pM level: miRNA-107, miRNA-122, and miRNA-141.

The reaction time of CHA also influenced the final result of ECL; after optimization, we set the CHA reaction time to 2 h (Figure 3B).

To demonstrate the successful fabrication of the biosensor, CV and electrochemical impedance spectroscopy (EIS) characterizations were performed in a solution containing 0.1 M KCl and 5 mM $[Fe(CN)_6]^{3-/4-}$. From Figure S11A, the bare GCE presented a well-defined redox peak (curve a). When the Pdots were dried on the surface of the electrode, the current decreased significantly owing to the hindrance of Pdots on electron transmission (curve b). After the immobilization of H_1 (curve b), MCH (curve c), report DNA (curve d), and H_2 (curve e) layer by layer, the peak current decreased gradually, suggesting that these biomolecules could hinder the diffusion of ferricyanide toward the electrode surface because of the electrostatic repulsion of $[Fe(CN)_6]^{3-/4-}$ from the electrode surface by the negative charges on the DNA strands. In addition, the EIS results also confirmed the CV findings. As shown in Figure S11B, the R_{et} of the modified GCE was increased gradually according to Figure S11A. The above-mentioned results meant that this biosensor had been successfully fabricated.

ECL Analysis of miRNA-21. Since the ECL intensity was related to the amount of H_2-BHQ controlled by miRNA-21, it was possible to quantitatively detect miRNA-21 by the difference of ECL intensity after incubation of H_2-BHQ. To evaluate the quantitative detection performance of miRNA-21 by the developed strategy, this proposed "ECL-RET" biosensor was used under the optimized conditions with varying concentrations of miRNA-21. As presented in Figure 4A, with the increase of the concentration of miRNA-21, the ECL intensity gradually decreased. In Figure 4B, it can be found that the ECL changes (ΔECL) were logarithmically related to the concentration of miRNA-21 ranging from 0.1 fM to 100 pM with the linear fitting equation $I = 24098.6 + 1387.4 \times \mathrm{Lg}\, C$ ($R^2 = 0.994$) (Figure 4B, inset). Also, the limit of detection (LOD) was calculated to be 32 aM (S/N = 3). The analytical performance parameters of the proposed biosensor including linear range and detection limit were compared with various reference methods. As shown in Table S4, the developed system displayed a wider linear range and a lower detection limit. Additionally, its detection performance was comparable with most reference methods, indicating that the proposed sensor provided a promising platform for detecting miRNA-21.

Reproducibility and Specificity of the ECL Sensor. The reproducibility of the ECL immunosensor with 1.0 pM miRNA-21 is displayed in Figure 4C. The RSD of five tests was 2.1%, demonstrating acceptable reproducibility and good precision. In addition, the selectivity of the biosensor for 1.0 pM miRNA-21 against a blank assay and other miRNA sequences at 10 pM levels of miRNA-107, miRNA-122, miRNA-141 was also explored. As exhibited in Figure 4D, the decrease in ECL signal was negligible for the blank and control assays, while a significant change appeared in the presence of the target miRNA-21. These results indicated that the proposed ECL biosensor has excellent selectivity.

CONCLUSIONS

In conclusion, we synthesized and prepared novel AIE-active Pdots with reversible redox properties, consisting of a tetraphenylethene derivate and BT, which displayed strong ECL signals in the aggregated states and good stability of ECL emission for annihilation, and reductive−oxidative, and oxidative−reductive modes. It was analyzed that the reason for the good stability of Pdots might be ascribed to its favorable redox reversibility, where the rigid structure of BT could retain its conjugated structure to great content in the aggregated states, benefiting to maintain the good electrochemical redox property. Based on the high ECL intensity and good stability of ECL emission, the Pdots were also applied in the ultrasensitive detection of miRNA-21 with a LOD of 32 aM. The Pdots with good ECL stability prepared in this work

https://doi.org/10.1021/acs.analchem.1c00947
Anal. Chem. 2021, 93, 6857−6864

not only open an avenue for the design of more excellent Pdots materials in the future but also help to broaden the application of Pdots in the field of biosensing.

■ ASSOCIATED CONTENT

Supporting Information

The Supporting Information is available free of charge at https://pubs.acs.org/doi/10.1021/acs.analchem.1c00947.

Materials, reagents, apparatus, ECL spectrum measurement, experiment of ECL imaging, ^{1}H NMR characterization, and absorbance spectra of the polymer; absorbance and PL lifetime spectra of Pdots; reductive−oxidative ECL of Pdots with $K_2S_2O_8$; corresponding CV and stability of ECL emission; CV of TPrA; polyacrylamide gel electrophoresis image; optimization of the kind and concentration of coreactants; CV and EIS profiles of the stepwise fabrications of the ECL sensor; sequences of DNA and miRNA used in this work; summarization of the photophysical characterization data for Pdots; and comparison of the ECL efficiency of different nanomaterials and analytical performance comparison of different methods for detection of miRNA-21 (PDF)

■ AUTHOR INFORMATION

Corresponding Authors

Jian-Bin Pan − *State Key Laboratory of Analytical Chemistry for Life Science, School of Chemistry and Chemical Engineering, Nanjing University, Nanjing 210023, China*; Email: jbpan@nju.edu.cn

Jing-Juan Xu − *State Key Laboratory of Analytical Chemistry for Life Science, School of Chemistry and Chemical Engineering, Nanjing University, Nanjing 210023, China*; orcid.org/0000-0001-9579-9318; Phone: +86-25-89687924; Email: xujj@nju.edu.cn

Authors

Nan Zhang − *State Key Laboratory of Analytical Chemistry for Life Science, School of Chemistry and Chemical Engineering, Nanjing University, Nanjing 210023, China*

Hang Gao − *State Key Laboratory of Analytical Chemistry for Life Science, School of Chemistry and Chemical Engineering, Nanjing University, Nanjing 210023, China*

Yi-Lei Jia − *State Key Laboratory of Analytical Chemistry for Life Science, School of Chemistry and Chemical Engineering, Nanjing University, Nanjing 210023, China*

Xi-Liang Luo − *Key Laboratory of Optic-electric Sensing and Analytical Chemistry for Life Science (MOE), College of Chemistry and Molecular Engineering, Qingdao University of Science and Technology, Qingdao 266042, China*

Hong-Yuan Chen − *State Key Laboratory of Analytical Chemistry for Life Science, School of Chemistry and Chemical Engineering, Nanjing University, Nanjing 210023, China*

Complete contact information is available at: https://pubs.acs.org/10.1021/acs.analchem.1c00947

Author Contributions

§N.Z. and H.G. contributed equally to this work. The manuscript was written through the contribution of all authors. All authors have given approval to the final version of the manuscript.

Notes

The authors declare no competing financial interest.

■ ACKNOWLEDGMENTS

The authors gratefully acknowledge the National Key R&D Program of China (Grant 2016YFA0201200), the National Natural Science Foundation of China (Grants No. 22034003), and the Excellent Research Program of Nanjing University (ZYJH004) for the support.

■ REFERENCES

(1) Mei, J.; Leung, N. L. C.; Kwok, R. T. K.; Lam, J. W. Y.; Tang, B. Z. *Chem. Rev.* **2015**, *115*, 11718−11940.

(2) Liu, Y.-X.; Wang, H.-H.; Zhao, T.-J.; Zhang, B.; Su, H.; Xue, Z.-H.; Li, X.-H.; Chen, J.-S. *J. Am. Chem. Soc.* **2019**, *141*, 38−41.

(3) Wang, F.; Fu, Y.; Ziffer, M. E.; Dai, Y.; Maehrlein, S. F.; Zhu, X. Y. *J. Am. Chem. Soc.* **2021**, *143*, 5−16.

(4) Xiong, J.-B.; Feng, H.-T.; Sun, J.-P.; Xie, W.-Z.; Yang, D.; Liu, M.; Zheng, Y.-S. *J. Am. Chem. Soc.* **2016**, *138*, 11469−11472.

(5) Huang, J.; Nie, H.; Zeng, J.; Zhuang, Z.; Gan, S.; Cai, Y.; Guo, J.; Su, S.-J.; Zhao, Z.; Tang, B. Z. *Angew. Chem., Int. Ed.* **2017**, *56*, 12971−12976.

(6) Jiang, M.-H.; Li, S.-K.; Zhong, X.; Liang, W.-B.; Chai, Y.-Q.; Zhuo, Y.; Yuan, R. *Anal. Chem.* **2019**, *91*, 3710−3716.

(7) Wu, Z.; Yao, Q.; Chai, O. J. H.; Ding, N.; Xu, W.; Zang, S.; Xie, J. *Angew. Chem., Int. Ed.* **2020**, *59*, 9934−9939.

(8) Niu, G.; Zheng, X.; Zhao, Z.; Zhang, H.; Wang, J.; He, X.; Chen, Y.; Shi, X.; Ma, C.; Kwok, R. T. K.; Lam, J. W. Y.; Sung, H. H. Y.; Williams, I. D.; Wong, K. S.; Wang, P.; Tang, B. Z. *J. Am. Chem. Soc.* **2019**, *141*, 15111−15120.

(9) Zhou, T.; Hu, R.; Wang, L.; Qiu, Y.; Zhang, G.; Deng, Q.; Zhang, H.; Yin, P.; Situ, B.; Zhan, C.; Qin, A.; Tang, B. Z. *Angew. Chem., Int. Ed.* **2020**, *59*, 9952−9956.

(10) Carrara, S.; Stringer, B.; Shokouhi, A.; Ramkissoon, P.; Agugiaro, J.; Wilson, D. J. D.; Barnard, P. J.; Hogan, C. F. *ACS Appl. Mater. Interfaces* **2018**, *10*, 37251−37257.

(11) Peng, H.; Huang, Z.; Deng, H.; Wu, W.; Huang, K.; Li, Z.; Chen, W.; Liu, J. *Angew. Chem., Int. Ed.* **2020**, *59*, 9982−9985.

(12) Han, Z.; Yang, Z.; Sun, H.; Xu, Y.; Ma, X.; Shan, D.; Chen, J.; Huo, S.; Zhang, Z.; Du, P.; Lu, X. *Angew. Chem., Int. Ed.* **2019**, *58*, 5915−5919.

(13) Yang, L.; Zhang, B.; Fu, L.; Fu, K.; Zou, G. *Angew. Chem., Int. Ed.* **2019**, *58*, 6901−6905.

(14) Yang, L.; Sun, X.; Wei, D.; Ju, H.; Du, Y.; Ma, H.; Wei, Q. *Anal. Chem.* **2021**, *93*, 1553−1560.

(15) Cui, L.; Zhao, M.-h.; Li, C.-c.; Wang, Q.; Luo, X.; Zhang, C.-y. *Anal. Chem.* **2021**, *93*, 2974−2981.

(16) Wei, X.; Zhu, M.-J.; Yan, H.; Lu, C.; Xu, J.-J. *Chem. - Eur. J.* **2019**, *25*, 12671−12683.

(17) Gao, H.; Zhang, N.; Li, Y.; Zhao, W.; Quan, Y.; Cheng, Y.; Chen, H.-Y.; Xu, J.-J. *Sci. China: Chem.* **2020**, *63*, 715−721.

(18) Gao, H.; Zhang, N.; Pan, J.-B.; Quan, Y.-W.; Cheng, Y.-X.; Chen, H.-Y.; Xu, J.-J. *ACS Appl. Mater. Interfaces* **2020**, *12*, 54012−54019.

(19) Carrara, S.; Aliprandi, A.; Hogan, C. F.; De Cola, L. *J. Am. Chem. Soc.* **2017**, *139*, 14605−14610.

(20) Wang, Z.; Pan, J.; Li, Q.; Zhou, Y.; Yang, S.; Xu, J.-J.; Hua, D. *Adv. Funct. Mater.* **2020**, *30*, No. 2000220.

(21) Wang, N.; Wang, Z.; Chen, L.; Chen, W.; Quan, Y.; Cheng, Y.; Ju, H. *Chem. Sci.* **2019**, *10*, 6815−6820.

(22) Pecher, J.; Mecking, S. *Chem. Rev.* **2010**, *110*, 6260−6279.

(23) Liu, J.-L.; Zhang, J.-Q.; Tang, Z.-L.; Zhuo, Y.; Chai, Y.-Q.; Yuan, R. *Chem. Sci.* **2019**, *10*, 4497−4501.

(24) Zhang, Y.; Song, J.; Qu, J.; Qian, P.-C.; Wong, W.-Y. *Sci. China: Chem.* **2021**, *64*, 341−357.

(25) Barłóg, M.; Zhang, X.; Kulai, I.; Yang, D. S.; Sredojevic, D. N.; Sil, A.; Ji, X.; Salih, K. S. M.; Bazzi, H. S.; Bronstein, H.; Fang, L.; Kim,

J.; Marks, T. J.; Guo, X.; Al-Hashimi, M. *Chem. Mater.* **2019**, *31*, 9488−9496.
(26) Wang, Y.; Liao, Q.; Chen, J.; Huang, W.; Zhuang, X.; Tang, Y.; Li, B.; Yao, X.; Feng, X.; Zhang, X.; Su, M.; He, Z.; Marks, T. J.; Facchetti, A.; Guo, X. *J. Am. Chem. Soc.* **2020**, *142*, 16632−16643.
(27) Omer, K. M.; Ku, S.-Y.; Cheng, J.-Z.; Chou, S.-H.; Wong, K.-T.; Bard, A. J. *J. Am. Chem. Soc.* **2011**, *133*, 5492−5499.
(28) He, Y.; Du, J.; Luo, J.; Chen, S.; Yuan, R. *Biosens. Bioelectron.* **2020**, *150*, No. 111898.
(29) Luo, J.-H.; Li, Q.; Chen, S.-H.; Yuan, R. *ACS Appl. Mater. Interfaces* **2019**, *11*, 27363−27370.
(30) Feng, Y.; Sun, F.; Wang, N.; Lei, J.; Ju, H. *Anal. Chem.* **2017**, *89*, 7659−7666.
(31) Ding, Z.; Quinn, B. M.; Haram, S. K.; Pell, L. E.; Korgel, B. A.; Bard, A. J. *Science* **2002**, *296*, 1293.
(32) Bae, Y.; Myung, N.; Bard, A. J. *Nano Lett.* **2004**, *4*, 1153−1161.
(33) Jadhav, T.; Dhokale, B.; Misra, R. *J. Mater. Chem. C* **2015**, *3*, 9063−9068.
(34) Ma, C.; Cao, Y.; Gou, X.; Zhu, J.-J. *Anal. Chem.* **2020**, *92*, 431−454.
(35) Wang, F.; Lin, J.; Zhao, T.; Hu, D.; Wu, T.; Liu, Y. *J. Am. Chem. Soc.* **2016**, *138*, 7718−7724.
(36) Zhang, N.; Gao, H.; Xu, C.-H.; Cheng, Y.; Chen, H.-Y.; Xu, J.-J. *Anal. Chem.* **2019**, *91*, 12553−12559.
(37) Xu, Z.-H.; Gao, H.; Zhang, N.; Zhao, W.; Cheng, Y.-X.; Xu, J.-J.; Chen, H.-Y. *Anal. Chem.* **2021**, *93*, 1686−1692.
(38) Huo, X.-L.; Zhang, N.; Yang, H.; Xu, J.-J.; Chen, H.-Y. *Anal. Chem.* **2018**, *90*, 13723−13728.
(39) Yin, B.-C.; Liu, Y.-Q.; Ye, B.-C. *J. Am. Chem. Soc.* **2012**, *134*, 5064−5067.
(40) Liu, C.; Chen, C.; Li, S.; Dong, H.; Dai, W.; Xu, T.; Liu, Y.; Yang, F.; Zhang, X. *Anal. Chem.* **2018**, *90*, 10591−10599.
(41) Xue, C.; Zhang, S.-X.; Ouyang, C.-H.; Chang, D.; Salena, B. J.; Li, Y.; Wu, Z.-S. *Angew. Chem., Int. Ed.* **2018**, *57*, 9739−9743.
(42) Jiang, Y.; Li, B.; Milligan, J. N.; Bhadra, S.; Ellington, A. D. *J. Am. Chem. Soc.* **2013**, *135*, 7430−7433.

https://doi.org/10.1021/acs.analchem.1c00947
Anal. Chem. 2021, 93, 6857−6864